Structural Engineering and Mechanics, *Vol. 71, No. 6 (2019) 643-656*
DOI: https://doi.org/10.12989/sem.2019.71.643

Verification of diaphragm seismic design factors for precast concrete parking structures

Dichuan Zhang*[1] and Robert Fleischman[2]

[1]*School of Engineering and Digital Science, Narzarbayev University*
[2]*Department of Civil Engineering and Engineering Mechanics, University of Arizona*

(Received August 22, 2018, Revised April 18, 2019, Accepted May 27, 2019)

Abstract. A new seismic design methodology was proposed for precast concrete diaphragms. This methodology adopts seismic design factors applied on top of current diaphragm design forces. These factors are aimed to produce diaphragm design strengths aligned with different seismic performance targets. These factors were established through extensive parametric studies. These studies used a simple evaluation structure with a single-bay rectangular diaphragm. The simple evaluation structure is suitable for establishment of the design factors over comprehensive structural geometry and design parameters. However, the application of the design factors to prototype structures with realistic layouts requires further verification and investigation. This paper presents diaphragm design of several precast concrete parking structures using the new design methodology and verification of the design factor through nonlinear dynamic time history analyses. The seismic behavior and performance of the diaphragm were investigated for the precast concrete parking structures. It was found that the design factor established for the new design methodology is applicable to the realistic precast concrete parking structures.

Keywords: precast concrete diaphragms; parking structures; nonlinear time history analysis; seismic design

1. Introduction

Precast concrete diaphragms have shown poor performance during major earthquakes. Especially in the 1994 Northridge earthquake, collapse of several precast concrete parking structures was due to failures of the diaphragm (Iverson and Hawkins 1994). Since then, understanding of the behavior of precast diaphragms has been steadily improved through extensive analytical and experimental research. It has been realized that the behavior of precast diaphragms is complex: (1) the inertial forces in diaphragms can be significantly higher than the one used in current design provisions (Rodriguez *et al*. 2002), even after yielding of the lateral force resisting system (LFRS) (Fleischman *et al*. 2002); (2) force paths in the diaphragm can be complicated (Wood *et al*. 2000); (3) most precast diaphragm reinforcement is under non-proportional combined axial and shear force (Lee and Kuchma 2008) (Farrow and Fleischman 2003) (Zhang *et al*. 2011); and (4) diaphragm flexibility can amplify inter-story drifts of the gravity columns far away from LFRS (Fleischman *et al*. 1998) (Fleischman and Farrow 2001) (Belleri *et al*. 2015).

A new seismic design methodology (DSDM TG 2014) (BSSC IT6 2014) was proposed for the precast concrete diaphragm and has been codified in ASCE-7 (2016) and Ghosh *et al*. (2017). This methodology is developed based on extensive analytical and experimental research (Fleischman *et al*. 2013). This methodology adopts seismic design factors applied on top of current diaphragm design forces (ASCE-7 2010). These factors are aimed to produce diaphragm design strengths aligned with different seismic performance targets. These factors were established through extensive parametric studies (Zhang and Fleischman 2016). These studies used a simple evaluation structure with a single-bay rectangular diaphragm.

The simple evaluation structure is suitable for establishment of the design factor over comprehensive structural geometry and design parameters. However, these design factors need to be validated for prototype structures with realistic layouts which have much more complicated force paths than the simple evaluation structure. The implementation of the design factor to the prototype structure requires further investigation. This paper presents diaphragm design of several precast concrete parking structures using the new design methodology and design factors. The design factors were evaluated for their applicability to the design of the precast concrete parking structure through nonlinear dynamic time history analyses. The seismic behavior and performance of the diaphragm were investigated for the precast parking structures.

2. Diaphragm design methodology

The design methodology aligns the diaphragm design force with performance targets under earthquakes (DSDM TG 2014). Three design options are available with different performance targets: (1) Elastic design option targets elastic diaphragm response at maximum considered earthquake (MCE); (2) Basic design option targets inelastic diaphragm

*Corresponding author, Assistant Professor
E-mail: dichuan.zhang@nu.edu.kz

http://www.techno-press.com/journals/sem&subpage=7
ISSN: 1225-4568 (Print), 1598-6217 (Online)

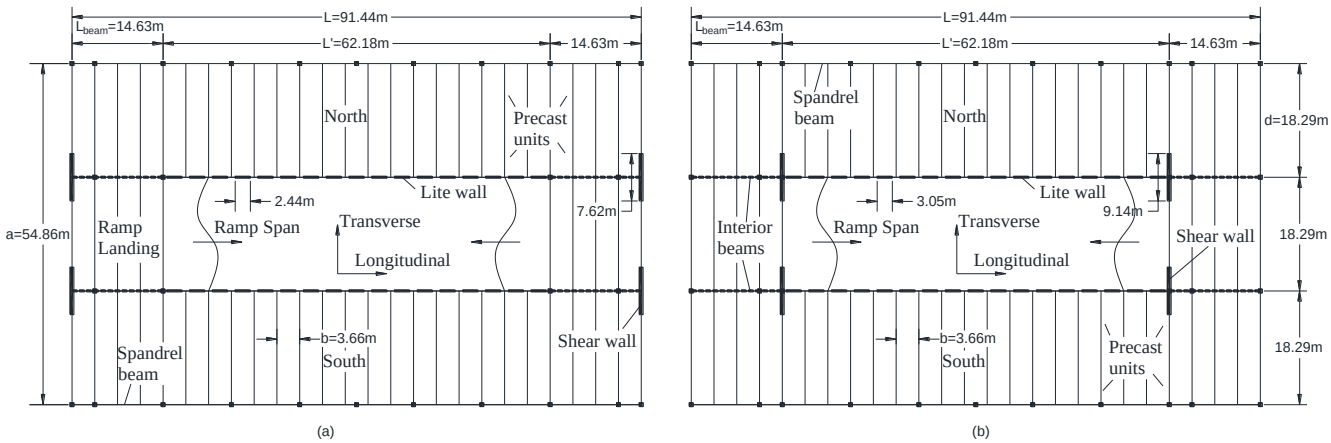

(a) Exterior shear wall (b) Interior shear wall for Seattle site

Fig.1 Plan of prototype structures

response at MCE with a maximum allowable deformation limit (5mm) in diaphragm reinforcement; and (3) Reduced design option targets inelastic diaphragm response at MCE with a maximum allowable deformation limit (10mm) in diaphragm reinforcement. The limits for the diaphragm reinforcement in basic and reduced design options were defined from a reliable deformation capacity exhibited in full-scale isolated diaphragm reinforcement tests (Ren and Naito 2013).

The performance targets are achieved by applying diaphragm force amplification factors (Ψ) on top of a baseline design force (F_D). The baseline design force is calculated from the current diaphragm design acceleration at top floor, F_{pn}/W_n, where F_{pn} is the diaphragm design force and W_n is the floor weight at top floor (ASCE-7 2010). The new design methodology uses different design patterns along the structural height for different types of buildings (DSDM TG 2014). For parking structures, the baseline force (F_D) is equal to W_nF_{pn}/W_n for top floor and 0.68 W_xF_{pn}/W_n for other floors, where W_x is the floor weight at floor x.

The diaphragm force amplification factors are defined as Ψ_E for elastic, Ψ_D for basic and Ψ_R for reduced design options. The equations for determining these factors have been developed in Zhang and Fleischman (2016)

Elastic:

$$\Psi_E = 1.75\ \Omega\ N^{0.35}[1-0.04(3.0-AR)^2] \geq 1.0 \quad (1a)$$

Basic:

$$\Psi_D = 1.75\ \Omega\ N^{0.20}[1-0.03(3.0-AR)^2] \geq 1.0 \quad (1b)$$

Reduced:

$$\Psi_R = 1.10\ \Omega\ N^{0.30}[1-0.03(2.5-AR)^2] \geq 1.0 \quad (1c)$$

where N is number of story (limited as 12), AR is diaphragm aspect ratio (limited as 4.0) and Ω is a factor considering the overstrength of the lateral force resisting system, which is calculated as

$$\Omega = 1 + 2.5\log\Omega_{LFRS} / N^{0.4} \quad (2)$$

where Ω_{LFRS} is the lateral force resisting system overstrength factor.

In addition to the diaphragm force amplification factor, a shear overstrength factor (Ω_v) is included in the design in order to preclude non-ductile failure modes (Zhang and Fleischman 2016). This factor is applied to the diaphragm design shear force obtained using the amplified diaphragm design force. It serves as a capacity design factor for the shear reinforcement. The shear overstrength factor can be determined as

Elastic: $\Omega_{vE} = 1.0$ (3a)

Basic: $\Omega_{vB} = 1.2 \leq 1.42AR^{-0.13} \leq 1.40$ (3b)

Reduced: $\Omega_{vR} = 1.5 \leq 1.92AR^{-0.18} \leq 1.96$ (3c)

3. Design of precast concrete parking structures

3.1 Selected precast concrete parking structures

Two precast Concrete parking structures were selected for evaluating the design methodology and diaphragm seismic response from a portfolio of prototype structures developed in Fleischman *et al*. (2005). The two selected structures are 4-story parking garages with exterior and interior shear wall layouts in the transverse direction respectively (See Fig. 1). Both structures have a footprint of 91.44 m x 54.86 m, resulting in three sub-diaphragms with 91.44 m×18.29 m of each. Precast diaphragm units are 3.66 m wide and are spanned in the transverse direction between spandrel beams and interior beams at ramp landing or lite walls at ramp span. The floor-to-floor height is 3.2 m for the typical floor and 4.88 m at the 1st floor. Both structures have thirty-four interior lite walls flanking the central ramp in the longitudinal direction and four shear walls in the transverse direction.

Table 1 Seismic design parameters

Site	S_{DS}	S_{D1}	SDC	Prototype structures	Lateral force resisting system		R	Ω_0	C_d
					Direction	Type			
Knoxville	0.45	0.16	C	Exterior shear wall	Transverse	Ordinary RC wall	5	2.5	4.5
					Longitudinal	Intermediate precast bearing wall	4	2.5	4
				Interior shear wall	Transverse	Ordinary RC wall	5	2.5	4.5
					Longitudinal	Intermediate precast bearing wall	4	2.5	4
Seattle	1.05	0.48	D	Interior shear wall	Transverse	Special RC wall	6	2.5	5
					Longitudinal	Special precast bearing wall	5	2.5	5

Table 2 Design of lateral force resisting system

Site	Direction	M_b (kN-m)	V_b (kN)	L_w (m)	t_w (m)	Quantity, m	M_{ns} (kN-m)	Ω_{LFRS}, $m\phi_f M_{ns}/M_b$
Knoxville	Transverse	73753	6770	7.62	0.305	4	20387	1.00
	Longitudinal	92192	8465	2.44	0.305	34	2999	1.00
Seattle	Transverse	188246	17357	9.14	0.305	4	52954	1.01
	Longitudinal	225896	20826	3.05	0.305	34	7517	1.02

3.2 Design of lateral force resisting system

The seismic design of the lateral system elements was based on the codes in place at the initiation of the study (ASCE-7 2010). Two seismic design sites were considered: Knoxville, KN representing a seismic design category C and Seattle, WA representing a seismic design category D. The exterior shear wall structure was designed for the Knoxville site. The interior shear wall structure was designed for both Knoxville and Seattle sites. The seismic design parameters are listed in Table 1. Nonlinear flexural response is assumed to be concentrated at the base of the wall. The shear wall base section is designed for bending moment, including the effects of the axial load from wall self-weight. The shear wall was designed to meet the required design strength (M_b) without overstrength at base ($\Omega_{LFRS} \approx 1.0$). The shear wall design is shown in Table 2.

3.3 Design of precast concrete diaphragm

The design of precast concrete diaphragm follows the new design methodology presented in Sec. 2. The diaphragm baseline design force (F_D) was first calculated for Knoxville and Seattle sites in two orthogonal directions as shown in Table 3. The floor weight at top floor is lower than other floors since only half of the ramp is included in the weight calculation of the top floor.

The diaphragm design factors were calculated using N=4 and Ω_{LFRS} =1.0 (see Table 2) by Eqn. 1 for Ψ and Eqn.3 for Ω_v. For exterior shear wall structure, the diaphragm aspect ratio AR=L/d=91.44/18.29=5.0 is larger than the limit in Eqn. 1; hence AR=4 was used. For interior shear wall structure, AR=L'/d=62.18/18.29=3.4. Five cases of diaphragm design were considered: three were considered for the exterior shear wall structure at Knoxville site using the three different design options; the other two were considered for the interior shear wall structure with the elastic design option for Knoxville site and the reduced design option for Seattle site. The calculated diaphragm design factors for all the five cases are shown in Table 4.

Table 5 shows the amplified diaphragm design force (ΨF_D) for two selected cases as examples. The design force was distributed into the sub-diaphragms (North, South and Ramp) using the tributary floor weight of each sub-diaphragm.

The diaphragm force transfer path could be much more complicated in the parking garage structure than the simple beam method used in the current design code (PCI 2004). Therefore, free body diagrams were developed to calculate the diaphragm internal forces (M_u, N_u and V_u) at each joint from the diaphragm design force (ΨF_D) obtained in Table 5. Table 6 shows the free body diagram and diaphragm internal force calculation equations for the north/south sub-diaphragm of the exterior shear wall structure loaded in the transverse direction as an example. The free body diagram was built by considering the force distribution and reactions at diaphragm boundaries. Similar free body diagrams and equations were developed for the exterior shear wall structure loaded in longitudinal direction and for the interior shear wall structure loaded in both directions (DSDM TG 2014). The diaphragm internal force was calculated independently for two orthogonal directions (transverse and longitudinal). The higher internal force between two directions was used for the diaphragm reinforcement design.

An interaction equation (Eqn. 4) considering combined effects of moment, axial and shear forces was used to size the diaphragm reinforcement to resist the diaphragm internal forces calculated from Table 6.

$$\sqrt{\left(\frac{|M_u|}{\phi_f M_n}+\frac{N_u}{\phi_f N_n}\right)^2+\left(\frac{\Omega_v V_u}{\phi_v V_n}\right)^2} \le 1.0 \qquad (4)$$

In Eqn. 4, ϕ_f and ϕ_v is strength reduction factor taken as 0.9 and 0.85 respectively (DSDM TG 2014). The shear overstrength factor (Ω_v) from Table 4 was used in Eqn. 4 to

Table 3 Calculation of diaphragm baseline design force (FD)

Site	Direction	F_{pn} (kN)	Floor weight Top, W_n (kN)	Floor weight Others, W_x (kN)	F_D (kN) Top floor	F_D (kN) other floors
Knoxville	Transverse	2144	24594	27779	2144	1647
	Longitudinal	2678	24594	27779	2678	2057
Seattle	Transverse	5894	24732	27917	5894	4524
	Longitudinal	7073	24732	27917	7073	5429

Table 4 Determination of diaphragm design factors

Prototype structure	Site	Ψ_E	Ψ_D	Ψ_R	Ω_{vE}	Ω_{vB}	Ω_{vR}
Exterior shear wall	Knoxville	2.73	2.24	1.55	1.0	1.20	1.50
Interior shear wall	Knoxville	2.82	-	-	1.0	-	-
	Seattle	-	-	1.63	-	-	1.54

Table 5 Amplified diaphragm design force

Prototype structure	Design Option	Direction	Floor	ΨF_D (kN) Total	ΨF_D (kN) North/South	ΨF_D (kN) Ramp
Exterior shear wall at Knoxville	Elastic	Transverse	Top	5851	2200	1452
			Others	4494	1498	1498
		Longitudinal	Top	7308	2747	1813
			Others	5613	1871	1871
Interior shear wall at Seattle	Reduced	Transverse	Top	9588	3605	2379
			Others	7359	2453	2453
		Longitudinal	Top	11506	4325	2855
			Others	8831	2944	2944

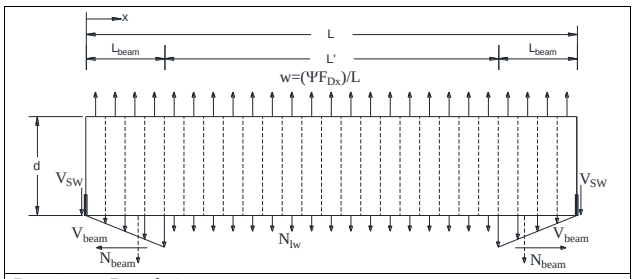

Reactions at Boundaries:

$$N_{lw} = 0.15w; \quad N_{Beam} = V_{SW} = 0.5(wL - N_{lw}L')/2$$

$$V_{beam} = 2w(L_{beam} + L')L_{beam}/3d$$

Internal Forces at Diaphragm Joints:

$0 \le x \le L_{beam}$:

$$N_u = xV_{beam}/L_{beam}; \quad V_u = V_{sw} - wx - xN_{beam}/L_{beam};$$

$$M_u = xV_{sw} - wx^2/2 - x^2 N_{beam}/3L_{beam}$$

$L_{beam} < x \le L/2$:

$$N_u = V_{beam}; \quad V_u = V_{sw} - wx - N_{beam} + N_{lw}(x - L_{beam});$$

$$M_u = xV_{sw} - wx^2/2 - N_{beam}(x - 2L_{beam}/3) + N_{lw}(x - L_{beam})^2/2$$

$L/2 < x \le L$:

Internal forces are symmetrical

Table 6 Example free body diagram and internal force calculation equations

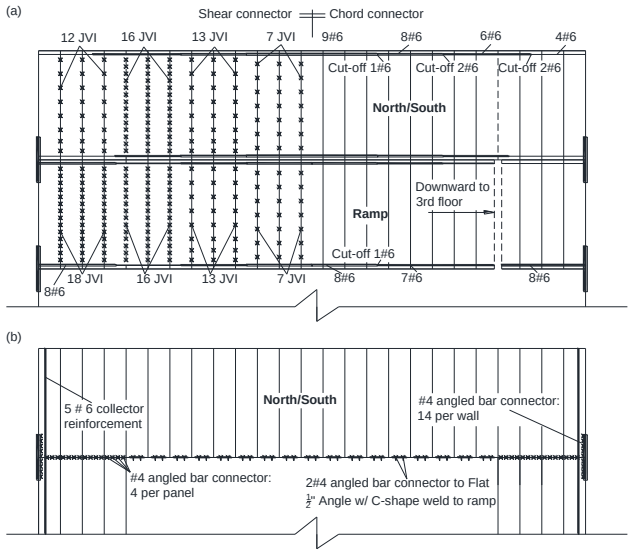

Fig. 2. Example diaphragm reinforcement at top floor: (a) primary; (b) secondary.

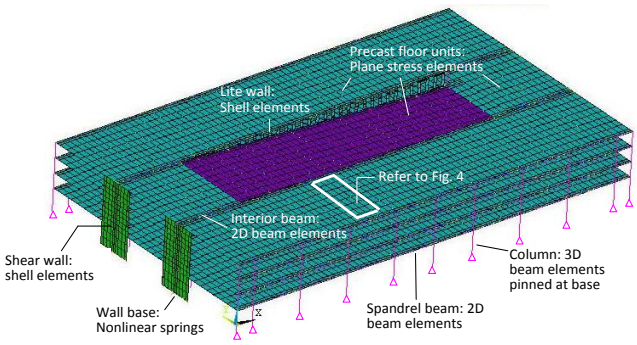

Fig. 3. 3D-FE model of the exterior shear wall structure

amplify the design shear force. The M_n, N_n and V_n are the nominal diaphragm joint moment, axial and shear strength calculated from the nominal axial and shear strength of diaphragm reinforcement (DSDM TG 2014). The diaphragm reinforcement contains chord connector to primarily resist the moment and axial force; and shear connector to primarily resist the shear force. In this study, pour strip chord (rebar in a cast-in-place strip) was selected as the chord connector. JVI Vector, a proprietary precast flange-to-flange connector, was selected as the shear connector. The nominal shear and axial strength of the pour strip chord and JVI vector were determined from the individual diaphragm connector tests (Naito and Ren 2013). As an example, the resultant diaphragm reinforcement detail is shown in Fig. 2a for the top floor of the exterior shear wall structure using the elastic design option.

Diaphragm secondary reinforcement, such as diaphragm to spandrel beam connector, diaphragm to interior beam connector, and diaphragm to wall connector, was also designed using Eqn. 4 with the reactions at boundaries of the free body diaphragm (See Table 6). Fig. 2b shows the diaphragm secondary reinforcement detail at the top floor for the exterior shear wall structure with the elastic design option as an example. As seen, #4 angled bar connectors were sized using Eqn. 4 in the most places except that

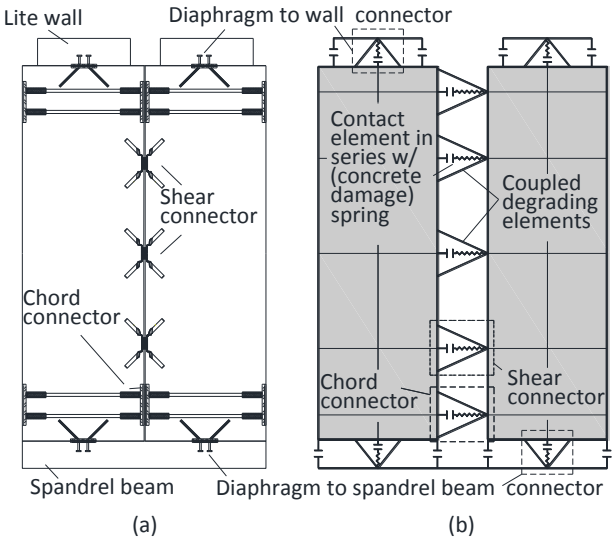

Fig. 4 Discrete connector model: (a) detail; (b) model.

Table 7 Information of ground motions

Site	EQ #	Earthquake	Magnitude	Scale factor	PGA (g) Trans. (y)	PGA (g) Long. (x)
Knoxville	KN1	Landers, USA, 1992	7.3	0.60	0.147	0.091
	KN2	Nahanni, Canada, 1985	6.8	0.35	0.352	0.394
	KN3	Tabas, Iran, 1978	7.4	0.58	0.234	0.189
Seattle	SE1	Cape Mendocino, USA, 1992	7.1	0.65	0.973	0.676
	SE2	Northridge, USA, 1994	6.7	0.60	0.506	0.363
	SE3	Western Washington, USA, 1979	7.1	2.00	0.560	0.329

flexible C-shape angles with slotted holes were selected for the ramp to lite wall connection. The C-shape angle permits relative sliding and opening deformation to mitigate the potential incompatible displacements of the ramp and the flat.

4. Analytical modeling

Nonlinear time history analysis (NLTHA) was performed using three-dimensional finite element (3D-FE) models of the prototype structure.

4.1 Prototype structure model

The 3D-FE model of the exterior shear wall structure is shown in Fig. 3. The interior shear wall has the similar model other than the position of the shear wall. The model was created using the general-purpose FE program ANSYS. The 3D-FE model includes all the elements presented in the structure including the primary (vertical plane) LFRS elements (shear wall or lite wall), gravity system columns, precast floor units, interior beams and spandrel beams on the floor system perimeter. These structural members were modeled as elastic elements: LFRS (wall and lite wall) was modeled as shell elements with cracked-section concrete properties; precast floor units were modeled as plane stress elements; and precast interior beams, spandrels and columns were modeled as beam/column elements with gross-section concrete properties due to the effects of prestressing. The nonlinear response was introduced through nonlinear springs at the base of the LFRS, and with discrete nonlinear connector elements in the diaphragm (refer to Sec. 4.2).

4.2 Discrete diaphragm model

Precast diaphragm behavior is highly dependent on the response of the connectors in the floor system and thus is not easily captured using the monolithic diaphragm models typically available in design office structural analysis packages, or smeared crack and concrete plasticity damage models widely used for modeling of nonlinear behaviors of other monolithic concrete members (Zhu *et al*. 2018) (Tulebekova *et al*. 2019). For this reason, discrete diaphragm models were developed for precast floor systems with connector elements placed at discrete locations along the diaphragm joint that directly represent the diaphragm connectors. The detailed model formulation is discussed in Wan *et al*. (2015) and Zhang *et al*. (2016). Each of the connectors between precast units was discretely modeled using an assemblage of nonlinear springs, links and contact elements (See Fig. 4) which possess tension-shear coupling and nonlinear cyclic-degrading effects (pinching, strength and stiffness degradation). Similar approach was also used for modeling of soil-structural interaction (Zhang et al. 2018). The model is based on a planar diaphragm model developed for nonlinear static "pushover" analysis (Fleischman and Wan 2007) and extended for NLTHA (Zhang *et al*. 2011). The properties used to construct the connector elements are determined on the basis of experimental data from full-scale physical tests of individual precast connectors (Ren and Naito 2013). Likewise, the calibration and validation of the models were based on physical testing, including hybrid (Zhang *et al*. 2011) and shake table tests (Schoettler *et al*. 2009) (Zhang *et al*., 2019).

4.3 Ground motions

The 3D-FE models were subjected to bi-directional earthquake inputs in transverse and longitudinal directions. Three historical ground motion pairs were selected for each site as shown in Table 7. The scaling of the ground motion pairs followed the ASCE-7 (Section 16.1.3.2) procedure: The average of the square root of the sum of squares (SRSS) 5% damping spectra does not fall below 1.3 times the corresponding ordinate of the design response spectrum by more than 10% for each period between 0.2T and 1.5T, where T is the fundamental period of structure. The SRSS response spectra of scaled ground motion pairs are shown in Fig. 5. As seen, the average of the SRSS response spectra meets the ASCE-7 requirement within the period range: $0.2T_{min}$ to $3.0T_{max}$, representing the minimum and maximum fundamental periods among the prototype structure designs. Between the two ground motion pairs, the stronger

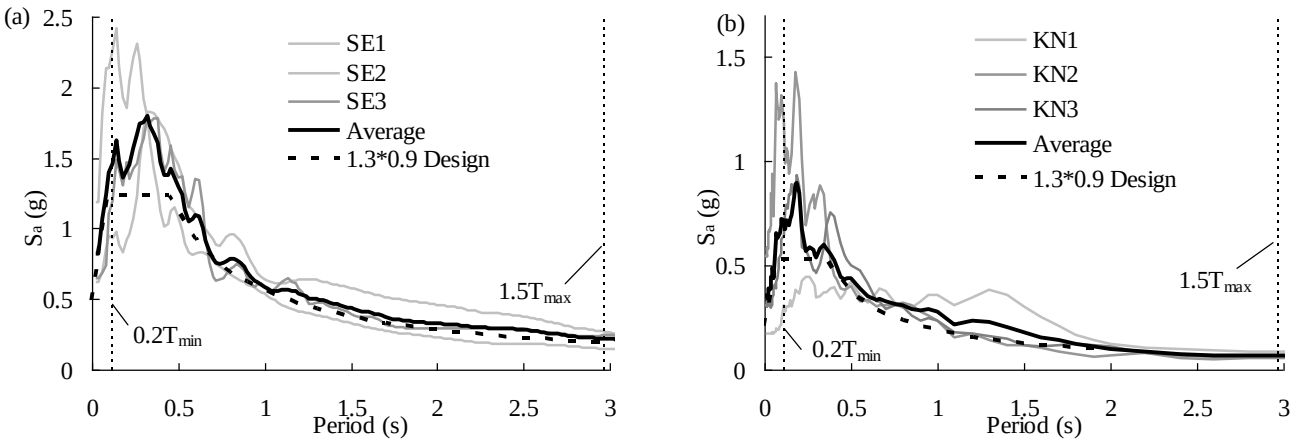

(a) Seattle (b) Knoxville

Fig. 5 5% damping SRSS response spectrum at design basis earthquake level.

component was applied in the transverse direction and the other component was applied in the longitudinal direction. This arrangement is to evaluate the most unfavorable condition since the seismic demands of the precast concrete diaphragm are mainly originated from the earthquake in the direction parallel to the precast panel, i.e. the transverse direction. The maximum demand from the three earthquake analyses at MCE was used to evaluate the prototype structure performance.

5. Analytical Results

This section presents the demand of diaphragm under the maximum considered earthquakes from the bi-directional earthquake simulations with comparisons to the design targets discussed in previous sections. The results presented in this section are the maximum of response from the three earthquake inputs.

5.1 Diaphragm inertial forces

Diaphragm inertial force is an important measurement for the diaphragm seismic design especially for the elastic design option. Diaphragm inertial force demands for two prototype structures (exterior and interior shear wall structures) at Knoxville site with elastic design option are discussed in this section.

Figure 6 shows the diaphragm total inertial force demand at each floor in (a) transverse and (b) longitudinal direction for the exterior shear wall structure. The envelope demand represents the maximum and minimum ever reached during the simulation and the profile demand represents instantaneous values at a time when top floor reaches the absolute maximum force. The amplified diaphragm design force from Table 5 is also indicated in the Fig. 6. As seen in Fig. 6, the diaphragm design force can safely cover the maximum diaphragm inertial force demand at all floor levels in both directions. In longitudinal direction, the diaphragm design force significantly overestimates the diaphragm inertial force because the smaller component of the ground motion pair was used in this direction. The profile demand showing a second mode response distribution indicates that the diaphragm response is controlled by the higher mode response rather than 1st mode, as previously observed in (Rodriguez *et al*. 2002).

Figure 7 shows the diaphragm inertial force envelope of each sub-diaphragm at each floor in the transverse direction for the exterior shear wall structure. The amplified diaphragm design force of each sub-diaphragm from Table 5 is also indicated in the Fig. 7. As seen in Fig. 7a, the design forces of north and south sub-diaphragms represent the diaphragm inertial force demand very well. The design force of ramp overestimates the diaphragm inertial force demand (See Fig. 7b) because of the uneven distribution of the diaphragm inertial force demand among sub-diaphragms.

Figure 8 shows the total diaphragm and north sub-diaphragm inertial force demand at each floor in the transverse direction for the interior shear wall structure. Similar trends and observations can be found in Fig. 8 as the exterior shear wall structure. Also noticed in Figs. 6-8, the diaphragm design force distribution along the building height can reasonably match the diaphragm inertial force envelope during the earthquake.

5.2 Diaphragm internal forces

The diaphragm internal force is evaluated in this section for the exterior shear wall structure designed with elastic design option and is compared to the design internal force from the free body diagram.

Figure 9 shows the diaphragm internal force in north sub-diaphragm (the most critical sub-diaphragm) at the top floor of the exterior shear wall structure. As seen in Fig. 9, the diaphragm has a complicated internal force distribution including significant axial (tension), moment and shear. The design force has a reasonable match to the demand from the earthquake simulations except that the earthquake simulation produces an asymmetrical distribution possibly due to non-uniform distribution of reactions between the diaphragm and lite wall. This asymmetrical distribution in

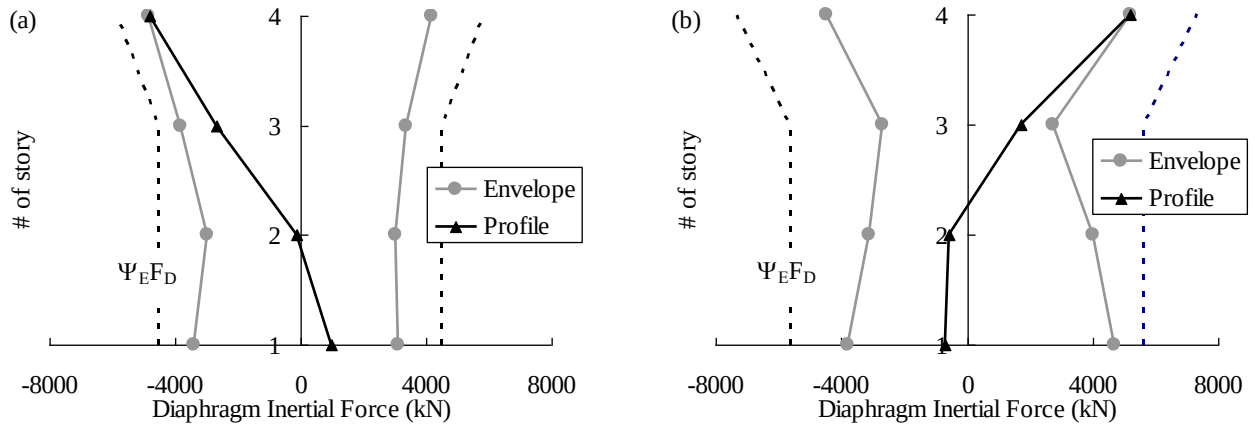

(a) Transverse direction (b) Longitudinal direction

Fig. 6 Diaphragm total inertial force demand of the exterior shear wall structure

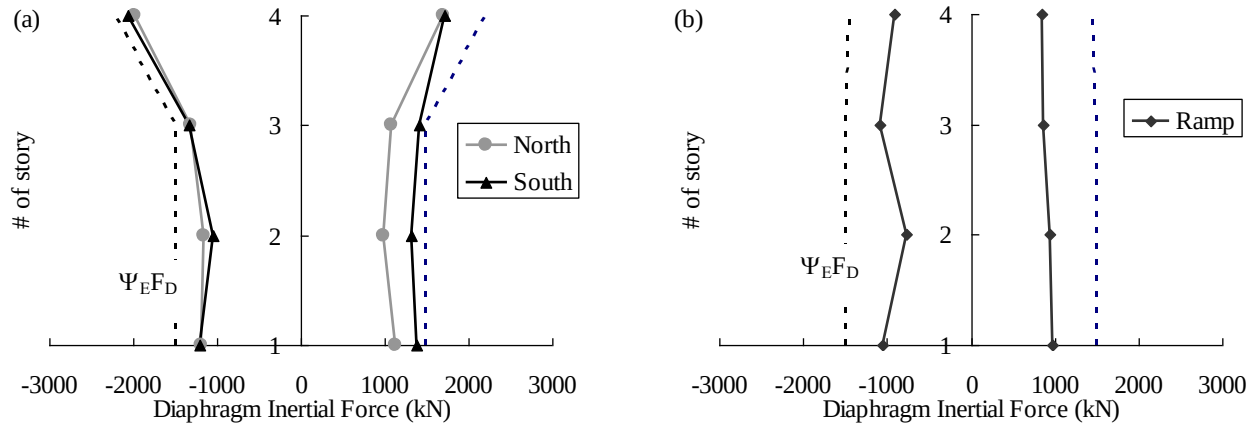

(a) North/south sub-diaphragms (b) Ramp

Fig. 7 Diaphragm inertial force envelope in the transverse direction of the exterior shear wall structure

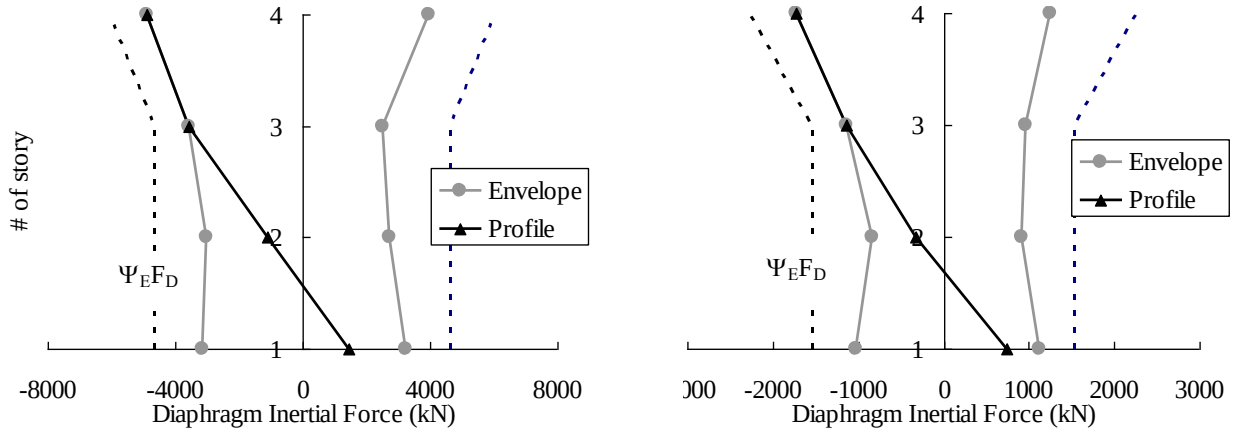

(a) Diaphragm total (b) North sub-diaphragm

Fig. 8 Diaphragm inertial force demand in the transverse direction of the interior shear wall structure

turn causes the design axial force overestimates but the design moment underestimates the diaphragm internal force demand for a half span. Since the diaphragm design includes combined effects of axial force and moment, the diaphragm overall performance in the simulation is still within the expected target (refer to Fig. 12).

Figure 10 shows the diaphragm internal force in the ramp at the top floor of the exterior shear wall structure. Similar complicated internal force distribution is observed in the ramp as the north sub-diaphragm. The design internal force from the free body diagram shows a reasonable match to the demand from the earthquake simulations.

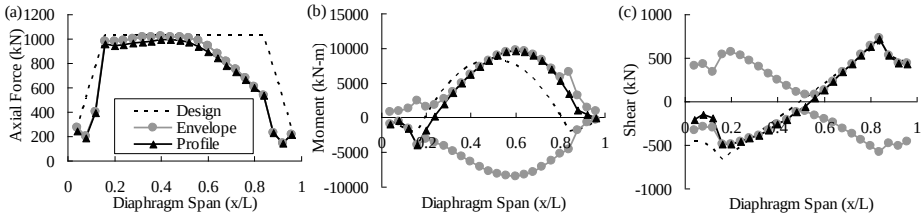

Fig. 9. Diaphragm internal force in north sub-diaphragm at top floor: (a) axial; (b) moment; (c) shear.

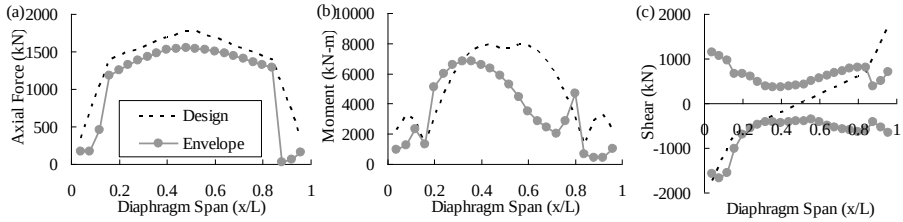

Fig. 10. Diaphragm internal force in ramp at top floor of the exterior shear wall structure: (a) axial; (b) moment; (c) shear.

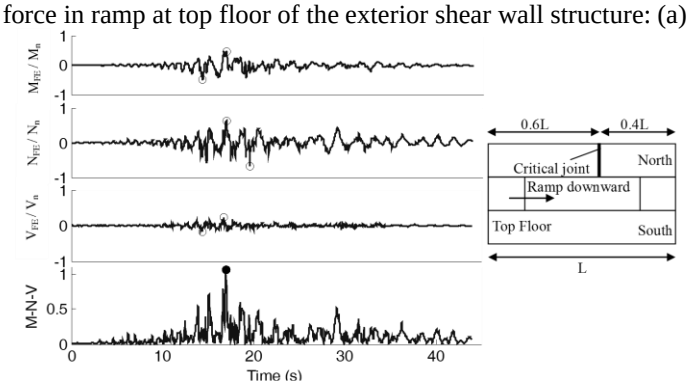

Fig. 11. Diaphragm internal force time history of the critical joint at top floor for the exterior shear wall structure.

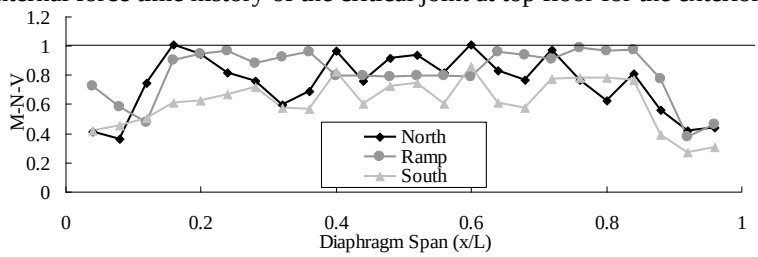

Fig. 12. Diaphragm internal force interaction (M-N-V) at top floor of the exterior shear wall structure.

A similar interaction calculation (See Eqn. 5) as the design interaction equation (Eqn. 4) was used to evaluate the combination of the diaphragm internal force demand discussed above. In Eqn.5, M_{FE}, N_{FE} and V_{FE} represent the maximum diaphragm internal force demand (moment, axial and shear) from the earthquake simulation. M_n, N_n and V_n represent the diaphragm design strength used in Eq. 4.

$$M-N-V=\sqrt{\left(\frac{|M_{FE}|}{M_n}+\frac{N_{FE}}{N_n}\right)^2+\left(\frac{V_{FE}}{V_n}\right)^2} \qquad (5)$$

Figure 11 shows the diaphragm internal force ratios between earthquake simulation demands and diaphragm joint nominal strength for each individual internal force and M-N-V interaction at a critical joint of the top floor of the exterior shear wall structure. Although the diaphragm individual internal force demands are considerably lower than the nominal strength, the combined effect of the diaphragm internal forces brings the joint close to its design strength (M-N-V reaching unity), though not repeatedly, during the earthquake.

Figure 12 shows the diaphragm internal force interaction (M-N-V) at top floor (the most critical floor) of the exterior shear wall structure designed with the elastic design option. As seen in Fig. 12, the interaction demand is under but close to 1.0, which indicates the validation of using Eqn.4 to consider the combined diaphragm internal force demand.

5.3 Diaphragm joint deformation

Diaphragm joint deformations are important measurement since they directly reflect the local deformation demand on the diaphragm reinforcement, especially for the basic and reduced design options where inelastic response is expected in the diaphragm reinforcement.

Figure 13 shows the maximum chord opening at all

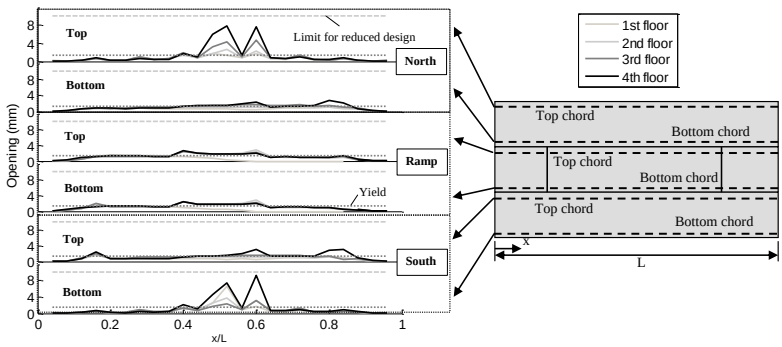

Fig. 13 Maximum chord opening for the interior shear wall structure designed with the reduced design option

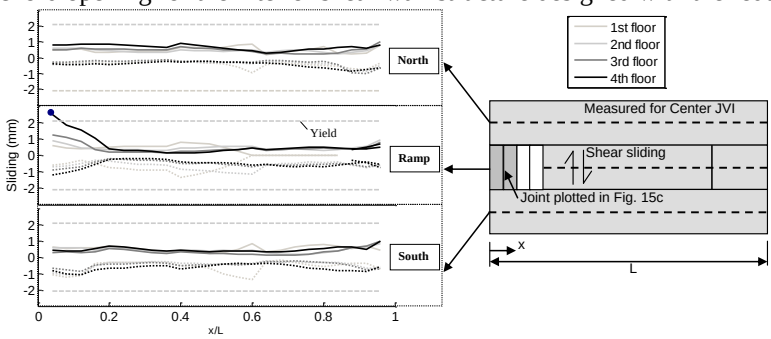

Fig. 14 Maximum JVI shear sliding for the exterior shear wall structure designed with the basic design option

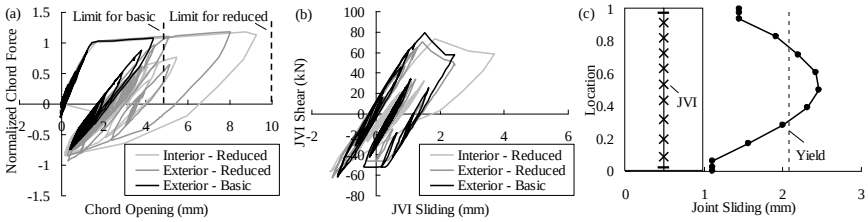

Fig. 15 Diaphragm reinforcement response: (a) chord in tension; (b) JVI in shear; (c) joint sliding

joints of all floors for the interior shear wall structure using the reduced design option. The yield opening and allowable limit for the reduced design are indicated as horizontal dotted and dashed lines respectively in the Figure. As seen in Fig. 13, the chord connector significantly yields at many locations but all connectors are safely within the allowable limit (10 mm) as expected from the design methodology. The larger demand occurs at the outer side of the north and south sub-diaphragms where the moment and axial (tension) forces are significant (refers to Fig. 9).

Figure 14 shows the maximum shear sliding at all joints at each floor level for the exterior shear wall structure designed with the basic design option. Although the chord reinforcement is allowed to yield in opening in basic and reduced design options, the shear sliding of shear connector (JVI) is expected to remain elastic during the earthquake for all design options. As seen in Fig. 14, all of joints exhibit a sliding demand less than the yielding sliding of JVI connector except for one joint in the flat region of ramp at top floor (see highlighted dot). This slightly exception is due to non-uniform distribution of shear sliding demand along the joint (refer to Fig. 15c). The connector was modeled with degradation behavior (see Fig. 15b). The joint seems can survive the earthquake without brittle failure under the help of other JVI connectors which still remain elastic. Therefore, the design seems acceptable.

Figure 15 shows the diaphragm reinforcement response for the most critical connector or joint. As seen in Fig. 15a, the chord connector has significant inelastic opening, but the maximum demand is less than the corresponding allowable limits for basic and reduced design option. Figure 15b shows inelastic sliding response in the JVI connector but the strength degradation is not significant. The inelastic sliding demand is due to the non-uniform distribution along the joint as shown in Fig. 15c.

5.4 Demands in diaphragm secondary reinforcement

Diaphragm secondary reinforcement connects diaphragm and other structural components including internal beams, spandrel beams, shear walls and lite walls. The new design methodology does not directly link the design to demand targets for the secondary reinforcement. However, the deformation demand of the secondary reinforcement needs to be limited within its deformation capacity.

Figure 16 shows deformation (opening and sliding) demand in the diaphragm secondary reinforcement at top floor for the exterior shear wall structure with the elastic

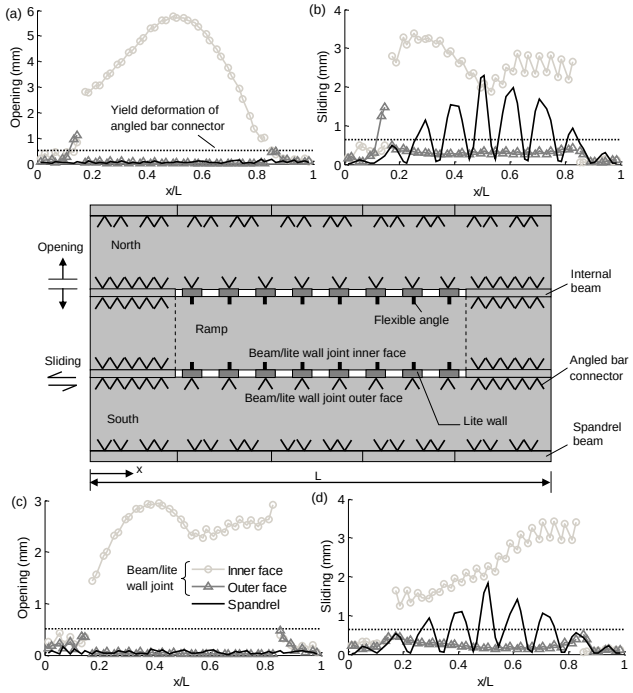

Fig. 16 Deformation demand in diaphragm secondary reinforcement at top floor: (a) opening at north; (b) sliding at north; (c) opening at south; (d) sliding at south

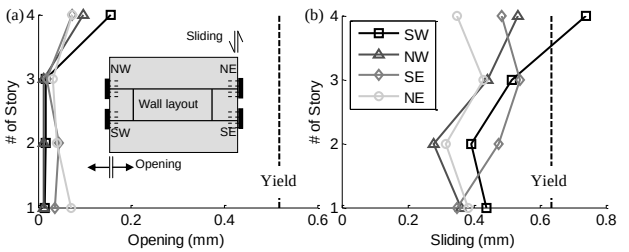

Fig. 17 Deformation demand in the diaphragm to wall connector for the exterior shear wall structure: (a) opening; (b) sliding.

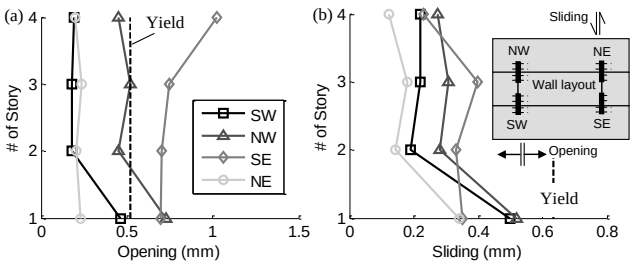

Fig. 18 Deformation demand in the diaphragm to wall connector for the interior shear wall structure: (a) opening; (b) sliding.

design option. The diaphragm secondary reinforcement presented in Fig. 16 includes the diaphragm to internal beam connector, the diaphragm to lite wall connector and the diaphragm to spandrel beam connector. The yield deformation of the angled bar connector is indicated as dotted line in the figure. As seen in Fig. 16, a couple of inelastic response is observed in the diaphragm secondary reinforcement even though the primary diaphragm reinforcement is designed to remain elastic (elastic design option).

Both opening and sliding demands grow for the diaphragm to internal beam connector as one moves inward along the internal beam (small demands near the exterior shear wall; large demands near the ramp termination). The reason for this trend is the nature of the end moment and shear flow actions across the joint between the diaphragm and internal beam due to the bending of the north flat sub-diaphragm, as was described previously in (Fleischman *et al*. 1998).

The north/south sub-diaphragm (outer side) to lite wall connection remains elastic while the ramp diaphragm (inner side) has large opening and sliding demand due to the use of the flexible C-shape angle. The opening response of diaphragm to spandrel beam connector remains elastic while the sliding demand exceeds the yield deformation to accommodate flexural deformation in the diaphragm span caused by the large moment and axial force, as discussed in (Wan *et al*. 2012).

Figure 17 shows the maximum deformation demand profile in the diaphragm to shear wall connector for the exterior shear wall structure with the elastic design option. As seen in Fig. 17a, the opening demands are significantly less than the connector yield opening. This implies that the lite walls successfully limit the orthogonal force demands on the wall, and that the out-of-plane flexibility of the shear wall is sufficient to limit the opening demands on the connector. As seen in Fig. 17b, the sliding deformation demands are within the elastic range at most locations except for the SW wall at the top floor (adjacent to the roof level down-ramp landing). This slight yielding is due to a non-uniform sliding distribution among the connectors as similarly observed in Fig. 15c.

Figure 18 shows the maximum deformation demand profile in the diaphragm to shear wall connector for the interior shear wall structure with the elastic design option. As seen in Fig. 18a, on the contrary to the exterior shear wall structure, the opening demands indicate some connectors are slightly yield in SE and NW wall due to combined (longitudinal) axial forces in the diaphragm and the in-plane negative moment acting on the wall. As seen in Fig. 18b, the sliding deformation demands are within the elastic range at all locations.

5.5 Design targets verification

This section presents the parametric results for different diaphragm design options to verify the design targets in the new design methodology.

Figure 19 shows the maximum demand of the diaphragm inertial force and the joint shear force. The diaphragm inertial force is normalized by the baseline design force (F_D, refer to Table 3). The joint shear force is normalized by the amplified design joint shear force (V_u, refer to Table 6) without the shear overstrength factor (Ω_v). The diaphragm force amplification factor (Ψ) and shear overstrength factor (Ω_v) are indicated as grey lines in Fig. 19a and 19b respectively.

As seen in Fig. 19a, the maximum diaphragm inertial force demand is higher than the force in current design code

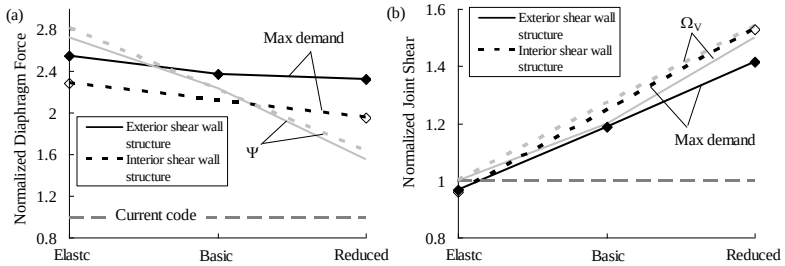

Fig. 19 Max diaphragm demands for different design options: (a) inertial force; (b) joint shear force.

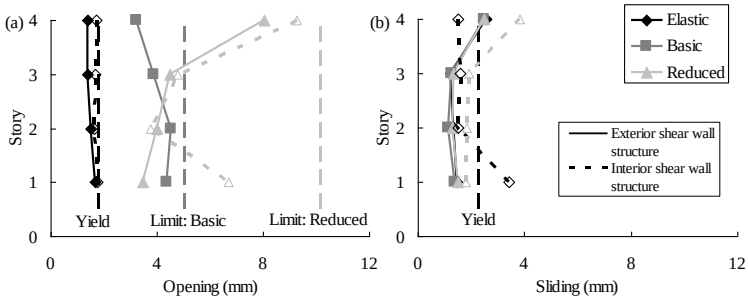

Fig. 20 Max joint deformation demand for different design options: (a) opening; (b) sliding.

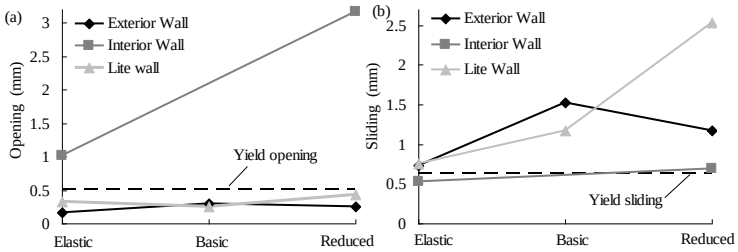

Fig. 21 Max joint deformation demand of the diaphragm to wall connector: (a) opening; (b) sliding.

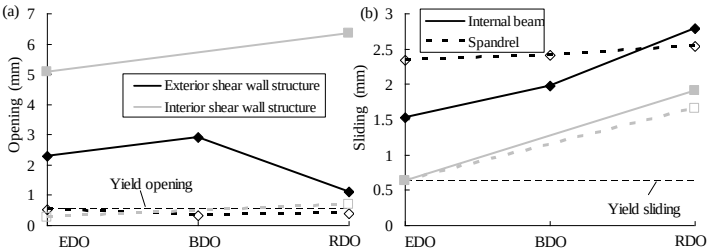

Fig. 22 Max joint deformation demand of the diaphragm to internal beam/spandrel beam connector: (a) opening; (b) sliding

for all cases. For the elastic design option, the amplified diaphragm design force is higher than the maximum demand as expected in the design target. For inelastic diaphragm design (basic and reduced design options), the maximum diaphragm inertial force is higher than the amplified diaphragm design force due to the strain hardening and plastic redistribution after the yielding of the diaphragm.

As seen in Fig. 19b, the maximum joint shear force is higher than the design shear force (V_u) without shear overstrength except for the elastic design option, which indicates the necessary of applying shear overstrength factors for basic and reduced design options. The proposed shear overstrength factors in the new design methodology effectively bound the maximum joint shear demand for the basic and reduced design options.

Figure 20 shows the maximum demand along the structural height of the diaphragm joint opening and sliding for different design options. The yield deformation and allowable limits are indicated as vertical dashed lines in the Figure. As seen in Fig. 20a, the diaphragm joint opening demand is less than the yielding opening for the elastic design option and is within the allowable limits for the basic and reduced design options. Figure 20a indicates that the diaphragm inelastic deformation design targets for the different design options are met during the earthquake simulations. As seen in Fig. 20b, the diaphragm sliding is slightly higher than the yield sliding at the top and bottom floors. This slightly yielding response in shear is not expected in the design targets. However, this response is caused by non-uniform distribution of the sliding along the joint as discussed in Section 5.3. The joint seems able to

redistribute and resist the shear demand without brittle failures as implied in Fig. 19b.

As discussed in Section 5.4, inelastic response is expected in the diaphragm secondary reinforcement even for the elastic design option. Figures 21 and 22 summarize the maximum opening and sliding demand in the diaphragm secondary reinforcement: diaphragm to wall connectors (See Fig. 21) and diaphragm to internal beam or spandrel beam connectors (See Fig. 22). It has been recommended in the design the new methodology that the diaphragm secondary reinforcement should possess inelastic deformation capacity not less than the value shown in Fig. 21 and Fig. 22 (DSDM TG 2014).

6. Conclusions

A new seismic design methodology was proposed for precast concrete diaphragms. This methodology adopts seismic design factors applied on top of current diaphragm design forces to produce diaphragm design strengths aligned with different seismic performance targets. This paper presents diaphragm design of several precast concrete parking structures using the new design factors and evaluates the validation of the design factor through nonlinear dynamic time history analyses. The seismic behavior and performance of the precast diaphragm were investigated for the precast concrete parking structures designed with the new design methodology.

The following conclusions can be made regarding the general behavior of the diaphragm observed in the earthquake simulations of the precast concrete parking structures: (1) diaphragm inertial force does not follow the 1st mode response distribution; the largest demand occurs at the top floor; (2) the force transfer path in the diaphragm is much more complicated than the simple beam theory used in the current design code; this complicated path results in combined axial, moment and shear forces in the diaphragm joint; (3) diaphragm inelastic joint opening demand spreads out among many locations; the largest demand is observed in the outer face of the north and south sub-diaphragms under the combined tension and moment; (4) the diaphragm can remain elastic in shear sliding in the most locations except that localized yielding of diaphragm joint under shear sliding is observed due to non-uniform distribution of the sliding demand along the joint; (5) inelastic deformation response is observed in the diaphragm secondary reinforcement at multiple locations even for the elastic design option.

The following conclusions can be made for the seismic performance of the diaphragm in precast concrete parking structures relative to the design targets in the new design methodology: (1) the diaphragm force amplification factors calculated from Eqn. 1 are able to fulfill the diaphragm design targets for different design options; (2) the diaphragm shear overstrength factors calculated from Eqn. 3 can prevent brittle shear failure in the diaphragm; (3) the proposed diaphragm design force distribution along the building height can reasonably represent the maximum diaphragm inertial force distribution under earthquakes; (3) the free body diagram method proposed in the new design methodology can reasonably catch the diaphragm internal forces under earthquakes; (4) the proposed interaction equation (Eqn. 4) is suitable for sizing the diaphragm reinforcement under combined axial, moment and shear forces; (5) it is recommended to impose deformation capacity requirement for the design of diaphragm secondary reinforcement.

Acknowledgments

This research was supported by the Precast/Prestressed Concrete Institute (PCI), the Charles Pankow Foundation, and the National Science Foundation (NSF) under Grant CMS-0324522 and SGER Supplement CMMI-0623952. The authors are grateful for this support. Any opinions, findings, and conclusions or recommendations expressed in this material are those of the author(s) and do not necessarily reflect the views of the National Science Foundation.

References

ASCE 7-10. (2010), Minimum Design Loads for Buildings and Other Structures. *American Society of Civil Engineers*.

ASCE 7-16. (2016), ASCE Minimum Design Loads and Associated Criteria for Buildings and Other Structures. *American Society of Civil Engineers*, USA.

Building Seismic Safety Council, Committee IT6 (2014), Precast Concrete Diaphragm Design. *Proposal IT06-002 - Revise ASCE/SEI 7-10 Sections 14.2.4, NEHRP*, USA.

Belleri, A., Torquati, M., Riva, P., and Nascimbene, R. (2015), "Vulnerability assessment and retrofit solutions of precast industrial structures", *Earthq. Struct.,* **8**(3), 801-820. http://dx.doi.org/10.12989/eas.2015.8.3.801.

DSDM Project Task Group (2014), Seismic Design Methodology Document for Precast Concrete Diaphragms, *Project 08-07 Research Product, Charles Pankow Foundation,* Virginia, USA.

Farrow K.T. and Fleischman R.B. (2003), "Effect of Dimension and Detail on the Capacity of Precast Concrete Parking Structure Diaphragms", *PCI J.*, **48**(5), 46-61.

Fleischman R.B. and Farrow K.T. (2001), "Dynamic Response of Perimeter Lateral-System Structures with Flexible Diaphragms", *Earthq. Eng. Struct. Dynam.,* **30**(5), 745-763.

Fleischman R.B., Farrow, K.T., Eastman K. (2002), "Seismic Response of Perimeter Lateral-system Structures with Highly Flexible Diaphragms", *Earthquake Spectra*, **18**(2), 251-286. https://doi.org/10.1193/1.1490547.

Fleischman, R.B., Naito C.J., Restrepo J., Sause R., Ghosh S.K., Wan G., Schoettler M., and Cao L. (2005), "Seismic design methodology for precast concrete diaphragms, Part 2: research program", *PCI Journal*, **51**(6), 2-19.

Fleischman R.B., Restrepo J.I, Naito C.J., Sause R., Zhang D. and Schoettler M. (2013), "Integrated Analytical and Experimental Research to Develop a New Seismic Design Methodology for Precast Concrete Diaphragms", *Special Issue of the ASCE Journal of Structural Engineering on NEES: Advances in Earthquake Engineering*, **V139**(7).

Fleischman, R.B., Sause, R., Pessiki, S. and Rhodes, A.B. (1998), "Seismic behavior of precast parking structure diaphragms", *PCI J.*, **43**(1), 38-53.

Fleischman, R.B. and Wan, G. (2007), "Appropriate overstrength of shear reinforcement in precast concrete diaphragms", *ASCE J. Struct. Eng.,* **133**(11), 1616-1626.

https://doi.org/10.1061/(ASCE)0733-9445(2007)133:11(1616).
Ghosh, S.K., Cleland, N.M., and Naito, C.J. (2017) "Seismic Design of Precast Concrete Diaphragms", *NEHRP Seismic Design Technical Brief No. 13*.
Iverson, J.K. and Hawkins, N.M. (1994), "Performance of Precast/prestressed Concrete Building Structures during Northridge Earthquake", *PCI J.*, **39**(2), 38-55. http://worldcat.org/oclc/12789822.
Lee, H.J. and Kuchma, D.A. (2008), "Seismic response of parking structures with precast concrete diaphragms", *PCI J.*, **53**(2), 71-94. http://worldcat.org/oclc/12789822.
Naito, C. and Ren, R. (2013), "An Evaluation Method for Precast Concrete Diaphragm Connectors Based on Structural Testing", *PCI J.*, **58**(2), 106-118.
Precast/Prestressed Concrete Institution (2004), *PCI Design Handbook: Precast and Prestressed Concrete*, Sixth Edition, Chicago, IL, USA.
Ren, R. and Naito, C. (2013), "Precast Concrete Diaphragm Connector Performance Database", *ASCE J. Struct. Eng.*,, **139**(1), 15-27. https://doi.org/10.1061/(ASCE)ST.1943-541X.0000598.
Rodriguez, M., Restrepo, JI. and Carr, A.J. (2002), "Earthquake Induced Floor Horizontal Accelerations in Buildings", *Earthq. Eng. Struct. Dynam.,* **31**(3), 693-718. https://doi.org/10.1002/eqe.149.
Schoettler, M.J., Belleri, A., Zhang, D., Restrepo, J. and Fleischman, R.B. (2009), "Preliminary results of the shake-table testing for development of a diaphragm seismic design methodology", *PCI J.*, **54**(1), 100-124.
Tulebekova S., Zhang, D., Lee, D., Kim, J., Barissov T., and Tsoy V. (2019) "Nonlinear Responses of Energy Storage Pile Foundations with Fiber Reinforced Concrete", *Struct. Eng. Mech.*, **71**(4), 363-375. https://doi.org/10.12989/sem.2019.71.4.363.
Wan, G., Fleischman, R.B. and Zhang, D. (2012), "Effect of spandrel beam to double tee connection characteristic of flexure-controlled precast diaphragms", *ASCE J. Struct. Eng.,* **138**(2), 247-258. https://doi.org/10.1061/(ASCE)ST.1943-541X.0000426.
Wan, G., Zhang, D., Fleischman, R.B., and Naito, C.J. (2015), "A Coupled Connector Element for Nonlinear Static Pushover Analysis of Precast Concrete Diaphragms", *Eng. Struct.*, **86**(1), 58-71. https://doi.org/10.1016/j.engstruct.2014.12.029.
Wood S.L., Stanton J.F. and Hawkins N.M. (2000), "New seismic design provisions for diaphragms in precast concrete parking structures", *PCI J.*, **45**(1), 50-65. http://worldcat.org/oclc/12789822.
Zhang, D., and Fleischman, R.B. (2016), "Establishment of performance-based seismic design factors for precast concrete floor diaphragms", *Earthq. Eng. Struct. Dynam.,* **45**, 675-698. https://doi.org/10.1002/eqe.2679.
Zhang, D., Fleischman, R.B., Naito, C., and Ren, R. (2011), **"**Experimental evaluation of pretopped precast diaphragm critical flexure joint under seismic demands", *ASCE J. Struct. Eng.,* **137**(10), 1063-1074. https://doi.org/10.1061/(ASCE)ST.1943-541X.0000352.
Zhang, D., Fleischman, R.B., Naito C.J. and Zhang, Z. (2016), "Development of Diaphragm Connector Elements for Three-Dimensional Nonlinear Dynamic Analysis of Precast Concrete Structures", *Adv. Struct. Eng.*, **19**(2), 187-202. https://doi.org/10.1177%2F1369433215624319.
Zhang, D., Fleischman, R.B., Schoettler, M.J., Restrepo, J.I. and Mielke, M. (2019), "Precast Diaphragm Response in a Half-Scale Shake Table Test", *ASCE J. Struct. Eng.,* **145**(5). https://doi.org/10.1061/(ASCE)ST.1943-541X.0002304.
Zhu H., Wan K.T., Satekenova E., Zhang, D., Leung, C. and Kim, J. (2018), "Development of lightweight strain hardening cementitious composite for structural retrofit and energy efficiency improvement of unreinforced masonry housings", *Construct. Build. Mater.*, **167**, 791-812. https://doi.org/10.1016/j.conbuildmat.2018.02.033.
Zhang, D., Kim, J., Tulebekova, S., Saliyev, D. and Lee, D.H. (2018), "Structural responses of reinforced concrete pile foundations subjected to pressures from compressed air for renewable energy storage", *J. Concrete Struct. Mater.,* **12**, 74. https://doi.org/10.1186/s40069-018-0294-z.

CC

Notations

AR	= diaphragm aspect (span to depth) ratio;
a	= depth of diaphragm;
b	= width of precast unit of the diaphragm;
c_d	= deflection amplification factor;
d	= depth of sub-diaphragm;
F_D	= diaphragm bas
F_{pn}	= diaphragm design force at top floor in current code;eline design force;
L	= diaphragm span;
L'	= diaphragm ramp span;
L_{beam}	= span of internal beam;
L_w, t_w	= depth, thickness of shear wall;
M_b	= design base moment of shear wall;
M_{FE}, N_{FE}, V_{FE}	= diaphragm joint internal moment, axial and shear force demand;
M_n, N_n, V_n	= diaphragm nominal joint moment, axial and shear strength;
M-N-V	= diaphragm joint demand under combined forces;
M_{ns}	= shear wall nominal flexural strength;
M_u, N_u, V_u	= diaphragm design internal moment, axial and shear forces;
m	= number of shear walls in plan;
N	= number of stories;
N_{beam}, V_{beam}	= diaphragm axial, shear reactions at the internal beam;

N_{IW}	= diaphragm axial reaction at the lite wall;
R	= response modification coefficient;
T	= fundamental period;
T_{min}, T_{max}	= minimum, maximum fundamental per iod of the prototype structure;
V_b	= design base shear of shear wall;
V_{SW}	= diaphragm shear reaction at the shear wall;
W_n	= floor weight at top floor;
W_x	= floor weight at floor x;
w	= distributed diaphragm design force;
ϕ_f, ϕ_v	= flexural, shear strength reduction factor;
Ω	= correction factor considering lateral force resisting system overstrength;
Ω_0	= System overstrength factor;
Ω_{LRFS}	= lateral force resisting system;
Ω_{VE},Ω_{VB},Ω_{VR}	=diaphragm shear overstrength factor for elastic, basic, reduced design options;
Ψ, Ω_V	=diaphragm force amplification, shear overstrength factor;
Ψ_E, Ψ_D, Ψ_R	=diaphragm force amplification factor for elastic, basic, reduced design options.